

# Range corrections for two-neutron halo nuclei in effective theory

David L. Canham\* and H.-W. Hammer†

*Helmholtz-Institut für Strahlen- und Kernphysik (Theorie)  
and Bethe Center for Theoretical Physics,  
Universität Bonn, 53115 Bonn, Germany*

(Dated: November 3, 2018)

## Abstract

The range corrections to the universal properties and structure of two-neutron halo nuclei are investigated within an effective quantum mechanics framework. Treating the nucleus as an effective three-body system, we make a systematic improvement upon previous calculations by calculating the linear range corrections at next-to-leading order. Since the effective ranges for the neutron-core interactions are not known, we estimate the effective range to be set by the inverse of the pion mass. We investigate the possibility of excited Efimov states in two-neutron halo nuclei and calculate their mean square radii to next-to-leading order. We find that the effective range corrections are generally small and the leading order predictions are very robust.

arXiv:0911.3238v2 [nucl-th] 25 Feb 2010

---

\*Electronic address: canham@hiskp.uni-bonn.de

†Electronic address: hammer@hiskp.uni-bonn.de

## I. INTRODUCTION

There is a considerable interest in the universal properties of physical systems with large scattering lengths [1–4]. The low-energy behavior of a few-body system with short-range interactions and scattering length  $|a|$  much larger than the range  $R$  of the underlying two-body interaction can be described in a model-independent way. This is achieved by formulating an effective theory that takes advantage of the separation of scales inherent in the system, thereby using the ratio  $R/|a|$  as a small expansion parameter. The theoretical uncertainty can then be systematically improved by including increasingly higher order terms in the expansion. These techniques can readily be applied to *halo nuclei*: a special class of nuclear systems consisting of a tightly bound core and a “halo” of lightly bound nucleons [5–8]. There is a growing history of studies which exploit the separation of scales found in halo nuclei to describe the system in an effective theory, assuming the core to be a structureless particle and treating the nucleus as a few-body system of core and valence nucleons [9–16].

In previous work [16], we explored the universal properties and structure of  $2n$  halo nuclei to leading order (LO) in the expansion in  $R/|a|$  by describing the halo nuclei as an effective three-body system consisting of a core and two lightly bound valence neutrons. We constructed an effective potential made up of two-body contact interactions, and showed that this approach is equivalent to an effective field theory (EFT) framework. Our main focus was the possibility of such three-body systems to display the universal Efimov effect [17]. Assuming the nuclear ground state to be an Efimov state, we confirmed earlier model studies showing that  $^{20}\text{C}$  is the only  $2n$  halo nucleus candidate to display an excited Efimov state [9, 10] if the  $^{19}\text{C}$  binding energy is less than 165 keV. We also calculated the properties of this state. Moreover, we studied the structure of other known halo nuclei, calculating the matter density form factors and mean square radii (See also Ref. [14] for a previous study).

In this paper, we improve upon our earlier calculation by including the momentum dependent next-to-leading order (NLO) term in the short-range effective potential. While the scattering of two particles at sufficiently low energy is determined to leading order by only the scattering length  $a$ , at NLO, the effective range  $r_0$  of the two-body interaction comes into play. Including the linear range correction, we should be able to predict low-energy observables up to errors of order  $(r_0/a)^2 \sim (M_{low}/M_{high})^2$ .

Effective field theories with contact interactions have already been used to study the NLO range corrections to various few-body systems with large scattering lengths, mostly focused on the three-nucleon system. The range corrections to S-wave neutron-deuteron scattering in the doublet channel were calculated in perturbation theory in Ref. [18]. In Refs. [19–21], low-energy three-body observables were calculated up to next-to-next-to-leading order (N<sup>2</sup>LO) using a formalism that partially resums higher-order range effects. An analysis of three- and four-body observables to NLO within the resonating group model was carried out in [22]. For a more exhaustive list of such higher-order studies in the three-nucleon system, see Refs. [3, 4] and references therein.

There has also been interest lately in calculating the effective range corrections to the Efimov effect for three identical bosons. Thøgersen et al. [23] focused on the range corrections for ultracold atoms caught in an optical trap. Platter, Ji, and Phillips have explored the corrections to the Efimov spectrum linear in  $r_0$  using once-subtracted momentum-space integral equations derived from effective field theory [24]. They showed that discrete scale invariance relates the relative corrections for different Efimov states and the bound state spectrum in the unitary limit is unaffected by the linear range corrections.

In this work, we focus on the NLO correction to the properties of two-neutron ( $2n$ ) halo nuclei arising from a non-zero effective range in the neutron-neutron and neutron-core interactions. In the next section, we discuss the theoretical framework for this extension. Our results are presented in Section III. We discuss the impact of this correction on the possibility of known  $2n$  halo nuclei to have an excited Efimov state and on their binding energies. Moreover, we calculate the shift in the mean square radii of various halo nuclei due to the non-zero effective range. Our conclusions are given in Section IV. Finally, some details on the derivation of the Wigner bound and the calculation of the matter form factors are given in the appendices.

## II. THEORETICAL FRAMEWORK

We want to extend the effective quantum mechanics framework used in Refs. [16, 25] to next-to-leading order (NLO). This formulation is equivalent to using field-theoretic language for the problem at hand. The short-range interactions characteristic of halo nuclei are described using an effective interaction potential. Using the NLO effective potential, the low-energy behavior of the system will be reproduced up to errors proportional to the low-momentum scale  $M_{low}$  over the high-momentum scale  $M_{high}$  squared. At this order, we require two coupling parameters  $C_0$  and  $C_2$  tuned to reproduce the scattering length  $a$  and effective range  $r_0$  of the two-body interaction. The theory is valid up to a momentum scale  $M_{high}$  at which the errors become of order one.

For the large separation of scales involved in halo nuclei, zero-range interactions can be used in constructing the effective interaction potential. This leads to a separable potential made up of contact interactions in a momentum expansion. The two-body S-wave NLO potential can be written as

$$\langle \vec{p} | V_{eff} | \vec{p}' \rangle = g(p)g(p')(C_0 + C_2(p^2 + p'^2) + \dots), \quad (1)$$

where the dots indicate higher order interactions and  $g(p)$  is a regulator function (sometimes called the form factor). Of course, the low-energy observables must be independent of the regularization scheme, and one can choose the scheme most convenient for calculations. For this study, we use a strong cutoff regularization, in which the effective potential is set to zero,  $V_{eff} = 0$ , for momenta  $p, p' > \Lambda$ . This corresponds to the regulator function  $g(p) = \theta(\Lambda - p)$  and allows for a simple inclusion of a three-body force term, as described below. A natural choice for the value of  $\Lambda$  is  $\Lambda \sim M_{high}$ , but observables are independent of  $\Lambda$  after renormalization, up to higher order corrections which scale with powers of  $1/\Lambda$ .

At this point it is worth commenting on the antisymmetry of the full wave function with respect to the exchange of nucleons in the core and the halo neutrons. In microscopic cluster models, such as the resonating group model [26] or fermionic molecular dynamics [27], the wave function is antisymmetric with respect to exchange of all nucleons. In our halo effective theory the wave function is only antisymmetric with respect to exchange of the halo nucleons since the nucleons in the core are not resolved. The error involved in this approximation is governed by the ratio of the binding momentum of the halo nucleons to the binding momentum of the core, i.e.  $M_{low}/M_{high}$ . Within the domain of validity of the effective theory such effects are subsumed in the effective range parameters of the neutron-core interaction and can be treated in perturbation theory. This can be understood as follows: The exchange of a nucleon from the core and a halo nucleon can only give a sizeable

contribution if there is a spatial overlap between the wave function of the core and the wave function of the halo nucleon. The overlap of the wave functions, however, is determined by the ratio  $M_{low}/M_{high}$ . If this ratio is of the order 1/3, one can expect the antisymmetrization effects to be 30% at leading order and 10% at next-to-leading order. For a microscopic study of antisymmetrization effects in the neutron-alpha system, see Ref. [28].

The potential (1) is then used in the solution of the three-body Faddeev equations in terms of the spectator functions  $F_i(q)$ , which represent the dynamics of the core ( $i = c$ ) and the halo neutron ( $i = n$ ). To find the bound state of a halo nucleus composed of two valence neutrons and a core with spin zero, the resulting coupled integral equations are simply a generalization of the three-boson equation<sup>1</sup> (see [25, 29] and references therein). In the remainder of the paper, we use units such that  $\hbar = c = 1$ . For convenience, we set the nucleon mass  $m = 1$ . The resulting integral equations for the spectator functions  $F_n(q)$  and  $F_c(q)$  and the bound state energy  $B_3 > 0$  are:

$$F_n(q) = \frac{1}{2} \int_0^\Lambda dq' q'^2 \left[ \left( \tilde{G}_n(q, q'; B_3) + \frac{H(\Lambda)}{\Lambda^2} \right) t_n(q'; B_3) F_n(q') \right. \\ \left. + \left( \tilde{G}_c(q, q'; B_3) + \frac{H(\Lambda)}{\Lambda^2} \right) t_c(q'; B_3) F_c(q') \right], \quad (2)$$

$$F_c(q) = \int_0^\Lambda dq' q'^2 \left[ \left( \tilde{G}_c(q', q; B_3) + \frac{H(\Lambda)}{\Lambda^2} \right) t_n(q'; B_3) F_n(q') \right]. \quad (3)$$

The functions  $\tilde{G}_c$  and  $\tilde{G}_n$  arise from the free three-body propagator. They are given by

$$\tilde{G}_n(q, q'; B_3) = \frac{A}{qq'} \ln \left( \frac{\frac{2A}{A+1} B_3 + q^2 + q'^2 + \frac{2}{A+1} qq'}{\frac{2A}{A+1} B_3 + q^2 + q'^2 - \frac{2}{A+1} qq'} \right), \quad (4)$$

$$\tilde{G}_c(q, q'; B_3) = \frac{1}{qq'} \ln \left( \frac{B_3 + q^2 + \frac{A+1}{2A} q'^2 + qq'}{B_3 + q^2 + \frac{A+1}{2A} q'^2 - qq'} \right), \quad (5)$$

where  $A$  is the number of nucleons in the core.

The effects of the interactions are contained in the two-body T-matrices which are obtained by solving the Lippmann-Schwinger equation for the neutron-neutron and neutron-core interactions with the effective potential in Eq. (1). In the kinematics of Eqs. (2, 3), we have for the neutron-core T-matrix:

$$t_n(q'; B_3) = \frac{A+1}{\pi A} \left( 1 - \tilde{E}_n(q'; B_3) h_{nc}(\tilde{x}_{nc}) \right) \left[ -\frac{1}{a_{nc}} f(\tilde{x}_{nc}) + \sqrt{\tilde{E}_n(q'; B_3)} \frac{2}{\pi} \arctan(\tilde{x}_n) \right. \\ \left. + h_{nc}(\tilde{x}_{nc}) \tilde{E}_n(q'; B_3) \left( \frac{2}{\pi} \Lambda - \sqrt{\tilde{E}_n(q'; B_3)} \frac{2}{\pi} \arctan(\tilde{x}_n) \right) \right]^{-1}, \quad (6)$$

---

<sup>1</sup> In fact, the equations are the same for any bound three-body system of two identical particles and a core with spin zero, which interact through the pair-wise zero-range potentials given in Eq. (1).

with

$$\tilde{E}_n(q'; B_3) = \frac{2A}{A+1} \left( B_3 + \frac{A+2}{2(A+1)} q'^2 \right), \quad (7)$$

and for the neutron-neutron T-matrix:

$$t_c(q'; B_3) = \frac{2}{\pi} \left( 1 - \tilde{E}_c(q'; B_3) h_{nn}(\tilde{x}_{nn}) \right) \left[ -\frac{1}{a_{nn}} f(\tilde{x}_{nn}) + \sqrt{\tilde{E}_c(q'; B_3)} \frac{2}{\pi} \arctan(\tilde{x}_c) \right. \\ \left. + h_{nn}(\tilde{x}_{nn}) \tilde{E}_c(q'; B_3) \left( \frac{2}{\pi} \Lambda - \sqrt{\tilde{E}_c(q'; B_3)} \frac{2}{\pi} \arctan(\tilde{x}_c) \right) \right]^{-1}, \quad (8)$$

with

$$\tilde{E}_c(q'; B_3) = B_3 + \frac{A+2}{4A} q'^2. \quad (9)$$

A single index  $n, c$  indicates the spectator particle and  $a_{nn}, r_{nn}$ , and  $a_{nc}, r_{nc}$  are the  $n$ - $n$  and  $n$ - $c$  scattering lengths and effective ranges, respectively. For brevity we have defined the variables:

$$\tilde{x}_i = \frac{\Lambda}{\sqrt{\tilde{E}_i(q'; B_3)}} \quad \text{and} \quad \tilde{x}_{ni} \equiv \frac{\Lambda}{\sqrt{2\mu E_{ni}}}, \quad \text{where } i = n, c. \quad (10)$$

Here,  $E_{ni}$  is the two-body bound (virtual) state energy calculated from the pole of the two-body T-matrix at NLO in the limit  $\Lambda \rightarrow \infty$ , with  $\mu$  the corresponding reduced mass. In this limit, which implies a cutoff much larger than the momentum scales involved in the problem:  $\Lambda \gg 1/|a|, \sqrt{\tilde{E}_i}, \sqrt{E_{ni}}$ , these T-matrices reproduce the usual effective range expansion at NLO. Therefore, the pole position can be found through the relation:

$$E_{ni} = \left( 1 - \sqrt{1 - 2r_{ni}/a_{ni}} \right)^2 / (2\mu r_{ni}^2). \quad (11)$$

At leading order ( $r_{ni} = 0$ ), this expression reduces to the universal formula for the two-body binding energy for systems with a large positive scattering length:  $E_{ni} = 1/(2\mu a_{ni}^2)$ . Moreover, we have simplified the expressions for the two-body T-matrices (6, 8) by defining the functions

$$f(\tilde{x}) = \frac{2}{\pi} \left( \arctan(\tilde{x}) + \frac{1}{\tilde{x}} \right), \quad (12)$$

which approaches one as  $\tilde{x}$  becomes large and

$$h_{ni}(\tilde{x}_{ni}) = \frac{1}{\Lambda^2} \frac{2 - \pi f(\tilde{x}_{ni}) \Lambda r_{ni} / 2}{2 - \pi f(\tilde{x}_{ni}) / (\Lambda a_{ni})}, \quad i = n, c, \quad (13)$$

which vanishes for large  $\tilde{x}_{ni}$ . The term proportional to  $h_{ni}(\tilde{x}_{ni}) \Lambda$  generates the effective range term in the two-body T-matrices (6, 8).

Finally, the dimensionless function  $H(\Lambda)$  is a short-range three-body force. This term was included in the integral equations (2, 3) in analogy to the three-boson case which our

equations reproduce in the limit of identical particles. It corresponds to a three-body contact interaction which is required for consistent renormalization [25, 30]. For a given value of  $\Lambda$ , the three-body term  $H$  can be tuned to reproduce a given three-body observable and then other low-energy observables can be predicted using the same value  $H$ . The running of the three-body force  $H(\Lambda)$  with the cutoff  $\Lambda$  is governed by a limit cycle. As a consequence, it is always possible to find a value of the cutoff  $\Lambda$  at which the three-body force vanishes. Hence, at leading order  $\Lambda$  can simply be used as the three-body parameter in practical calculations [31]. The correct renormalization in the effective theory was explicitly verified [25]. Apart from the three-body observable, our input parameters at NLO are the  $n$ - $c$  and  $n$ - $n$  scattering lengths (or energies) and the corresponding effective ranges. The three-body binding energies are then given by the values of  $B_3$  for which the coupled integral equations (2, 3) have a nontrivial solution.

For most halo nuclei, the  $n$ - $c$  scattering length is not as well known as the two-body bound (virtual) state energy. Therefore, we will generally use the two-body energy  $E_{nc}$  as an input parameter. From  $E_{nc}$  and  $r_{nc}$ , we can calculate the corresponding  $a_{nc}$  to be used in the two-body T-matrices through Eq. (11). The  $n$ - $c$  effective ranges for most halo nuclei are not known experimentally. However, the range of the interaction between two nucleons is determined by the exchange of pions. We therefore use the inverse of the pion mass,  $m_\pi = 140$  MeV, to estimate the  $n$ - $c$  effective range,  $r_{nc} \approx 1/m_\pi = 1.4$  fm. This is equivalent to setting the effective range to the natural low-energy length scale of the system. The value of the  $n$ - $n$  effective range is known experimentally:  $r_{nn} = (2.75 \pm 0.11)$  fm [32]. Its size is comparable to the inverse of the pion mass scale. In our numerical calculations we use  $r_{nn} \approx r_{nc} \approx 1/m_\pi = 1.4$  fm. This choice is sufficient for our purpose of estimating the size of the range corrections and testing the robustness of the leading order results. Moreover, it allows a slightly larger range of cutoffs to be consistent with the Wigner bound.

The Wigner bound is based on general arguments and constrains the value of the effective range that can be generated by short-range potentials. It has been shown that the renormalization of an effective potential made up of contact interactions in a momentum expansion can only be performed if certain constraints are placed on the effective range [33]. More specifically, the effective range must be negative in the zero-range limit of the potential. In our case, this corresponds to the limit  $\Lambda \rightarrow \infty$  since a finite cutoff generates a finite range. This constraint follows directly from a general bound on the derivatives of the phase shifts derived first by Wigner in 1954 [34]. Wigner derived this bound from the fundamental principles of causality and unitarity, holding that a scattered wave cannot leave the scatterer before the incident wave has reached it. Phillips and Cohen derived the relation between the Wigner bound on the derivatives of phase shifts with the constraint on the effective range for short-range potentials [35]. This bound applies even if the potential does not vanish exactly outside some finite radius but merely decreases fast enough for the wave function to approach the asymptotic solution sufficiently quickly. The Wigner bound for zero-range potentials was shown to hold true no matter how many terms in the momentum expansion are included in the potential [33]. A very recent study has generalized the Wigner Bound to arbitrary dimension and angular momentum [36]. An explicit derivation of the Wigner bound constraint for our effective potential is given in Appendix A. In our numerical results in the next section, the cutoff is always chosen in accordance with the Wigner bound.

### III. EFFECTIVE RANGE CORRECTIONS TO $2n$ HALO NUCLEI

In this section we present numerical results for the effective range corrections to low-energy observables of three-body halo nuclei composed of a core and two valence neutrons. We begin with the range corrections to the possibility of the Efimov effect in  $2n$  halo nuclei, as well as to the binding energy of a possible Efimov excited state in  $^{20}\text{C}$ . After that, we estimate and discuss effective range corrections to the mean square radii results.

#### A. Range Corrections to $2n$ Halo Nuclei Binding Energies

In Ref. [16], we have calculated boundary curves representing the existence of an excited Efimov state for various values of the core mass in the parametric region defined by the ratios  $(E_{nc}/B_3^{(n)})^{1/2}$  versus  $(E_{nn}/B_3^{(n)})^{1/2}$ , where  $E_{nc}$  and  $E_{nn}$  are the  $n$ - $c$  and  $n$ - $n$  two-body energies related to the S-wave scattering length to LO. An analogous study was carried out previously in Ref. [10] within the renormalized zero-range model and motivated our investigation. It should be noted, however, that this type of analysis implicitly assumes that the ground state of a halo nucleus is an Efimov state. More general scenarios where only the excited state has universal character cannot be excluded. The curve itself is built up of the points for which the  $B_3^{(n+1)}$  binding energy is equal to the scattering threshold. This is equivalent to finding the critical scattering lengths of the three-body system. In similar studies looking at the range corrections to the Efimov effect in the three-boson system [23, 24], it was observed that including a non-zero effective range shifted the positions of the critical scattering lengths. However, for all values of effective ranges  $r_{nc}$  and  $r_{nn}$  within the range of validity of our effective theory ( $r_{ni} \ll |a_{ni}|$ ,  $i = n, c$ ), we find these shifts to be extremely small such that the boundary curves calculated with a non-zero effective range are indistinguishable from those at LO (See Fig. 2 of Ref. [16]).

As a consequence, the main conclusion from [16] is only slightly changed by the NLO range corrections: if the  $n$ - $^{18}\text{C}$  bound state energy satisfies  $E_{nc} < 161$  keV,  $^{20}\text{C}$  will have an excited Efimov state. In the following, we investigate the dependence on the  $n$ - $^{18}\text{C}$  bound state energy in more detail. In Ref. [16], we calculated the value of the possible excited state energies at LO as a function of  $E_{nc}$ , using the standard value for  $a_{nn} = (-18.7 \pm 0.6)$  fm [37], and fixing the cutoff  $\Lambda$  to reproduce the experimental value of the ground state energy  $B_3^{(0)} = 3506$  keV [38, 39]. Now using the estimate  $r_0 = r_{nn} = r_{nc} \approx 1/m_\pi = 1.4$  fm for the effective ranges along with the standard value for  $a_{nn}$  given above, we calculate the excited state energies  $B_3^{(1)}$  as a function of  $E_{nc}$  to NLO, by fixing  $\Lambda$  and tuning the three-body term  $H$  to reproduce the experimental value of the ground state energy  $B_3^{(0)} = 3506$  keV. For our calculations we use the cutoff  $\Lambda = 580$  MeV. The NLO result is compared to the LO result in Fig. 1, where the solid black line is the excited state energy to LO, the dotted-dashed red line to NLO, and the dashed line represents the scattering threshold. The inset graph shows the excited state energy relative to the scattering threshold. Whereas the excited state in the LO calculation exists when  $E_{nc} < 165$  keV, the state to NLO only exists when  $E_{nc} < 161$  keV. For larger values of  $E_{nc}$ , the  $^{20}\text{C}$  system moves across the scattering threshold, and the excited Efimov state disappears. We also see that the effective range corrections only lead to a recognizable shift toward smaller binding energies for  $E_{nc} < 90$  keV. For larger values of  $E_{nc}$  there is a region where the effective range corrections lead to a shift towards larger binding energies. However, this shift is always very small, no greater than  $\approx 0.5$  keV over

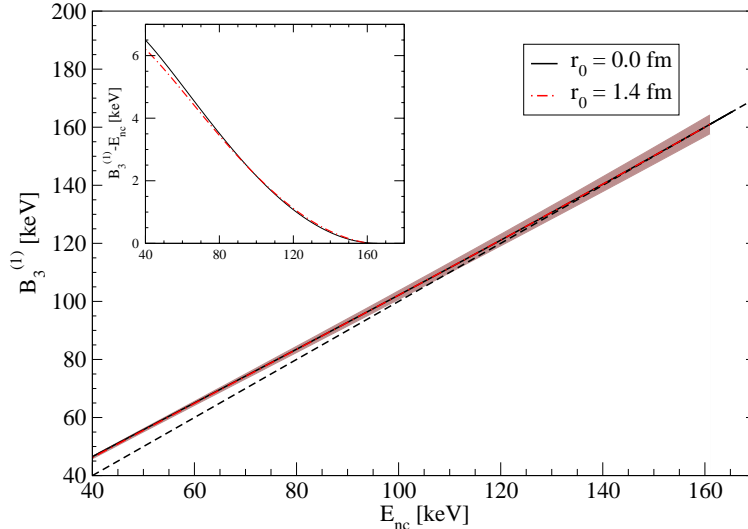


FIG. 1: Binding energy of the  $^{20}\text{C}$  excited Efimov state as a function of the  $n$ - $^{18}\text{C}$  bound state energy to LO (solid black line) and NLO (dotted-dashed red line) with NLO error bands. The dashed line represents the scattering threshold which is given by  $B_3^{(1)} = E_{nc}$ . The inset shows the excited state energy relative to the scattering threshold.

the whole range of possible  $E_{nc}$  values shown, and always smaller than the NLO error bands.

We have estimated this NLO error using the theoretical uncertainty of our effective potential. The uncertainty in binding energies calculated using the two-body effective potential of Eq. (1) is  $\approx (r_0/a)^2$ . For effective ranges much smaller than the scattering length we know that  $1/a_{nc}^2 \approx 2\mu_{nc}E_{nc}$ . Therefore, we estimate the theoretical uncertainty in the binding energy of the excited state using the sum of the uncertainties from the  $n$ - $n$  and  $n$ - $^{18}\text{C}$  interactions:  $\Delta B_3^{(1)}/B_3^{(1)} \approx (r_{nn}/a_{nn})^2 + r_{nc}^2(2\mu_{nc}E_{nc})$ .

The TUNL nuclear data evaluation from 1995 [38, 39] quotes the  $n$ - $^{18}\text{C}$  bound state energy as  $E_{nc} = (162 \pm 112)$  keV. This value is based on experiments using strong breakup reactions [40–43] and would leave the possibility of an Efimov excited state in  $^{20}\text{C}$  open. The more recent atomic mass evaluation AME2003 [44], however, quotes  $E_{nc} = (580 \pm 100)$  keV which excludes an excited Efimov state. This evaluation includes a recent measurement of  $E_{nc}$  using Coulomb dissociation of  $^{19}\text{C}$  that found  $E_{nc} = (530 \pm 130)$  keV [45]. Typel and Baur showed that the value of Ref. [45] is also consistent the distribution of the  $B(E1)$  continuum strength [46]. A review of the experiments was given in [47].

## B. Range Corrections to $2n$ Halo Nuclei Mean Square Radii

In this subsection, we will calculate the NLO corrections to the mean square radii of  $2n$  halo nuclei. We will briefly review the necessary formalism and then present our results. A more detailed description of the formalism is given in Refs. [16, 29]. For the calculation of the one- and two-body matter density form factors and mean square radii, we need the full three-body wave function, which can be reconstructed from the Faddeev spectator functions  $F_n$  and  $F_c$ . The relevant formulae are given in Appendix B.

The mean square radii are then calculated from the matter density form factors in the



low momentum transfer region, where the slope of the form factor determines the mean square radius  $\langle r^2 \rangle$ :

$$\mathcal{F}(k^2) = 1 - \frac{1}{6}k^2 \langle r^2 \rangle + \dots \quad (14)$$

Of course, the mean square radius acquired depends on the choice of one- or two-body form factor. These matter density form factors are calculated from the full wave function of the three-body system through Eqs. (B8, B9, B10). The slope of the two-body form factor  $\mathcal{F}_{ni}(k^2)$ , where  $i = n, c$ , will give the mean square distance between the two particles in the chosen two-body subsystem, either  $\langle r_{nn}^2 \rangle$  or  $\langle r_{nc}^2 \rangle$ . Analogously, the slope of the one-body form factor  $\mathcal{F}_i(k^2)$  will give the mean square distance of the spectator particle from the center of mass of the two-body subsystem, either  $\langle r_{c-nn}^2 \rangle$  or  $\langle r_{n-nc}^2 \rangle$ . However, it is more useful to calculate the distance of the individual particles from the center of mass of the three-body bound state. If  $b_i$  is the slope of the one-body form factor  $\mathcal{F}_i(k^2)$  at  $k^2 = 0$ , the mean square radius of one of the bodies  $i$  from the three-body center of mass is given by:

$$\langle r_i^2 \rangle = -6b_i \left( 1 - \frac{m_i}{2m_n + m_c} \right)^2, \quad (15)$$

where  $m_i$  is the mass of the desired constituent,  $i = n, c$ , and  $m_n$  and  $m_c$  are the neutron and core masses, respectively.

We have extracted the radii by fitting a polynomial in  $k^2$  to the form factor results for small  $k^2$ . We have used polynomials of varying degree up to 5th order in  $k^2$  in order to verify the stability and convergence of the fit. We have found a satisfactory stability in the slope when fitting to a polynomial to the fourth order in  $k^2$ , up to a value of  $k^2$  at which the form factor has dropped less than 10 percent.

The extracted radii for known halo nuclei to both LO and NLO are shown in Table I. We show only a selection of the LO results found in Ref. [16], to give a general overview of NLO corrections to the LO results. As input we have used the standard value of the  $n$ - $n$  scattering length,  $a_{nn} = (-18.7 \pm 0.6)$  fm [37], along with the experimental values of the  $n$ - $c$  two-body energies  $E_{nc}$  shown in the third column of Table I (negative values correspond to virtual energies). The effective range of both two-body subsystems is shown in the fourth column, indicating which results refer to LO ( $r_0 = 0$  fm) or NLO ( $r_0 = 1.4$  fm) calculations. As before, we use the inverse of the pion mass to estimate the effective range of both the  $n$ - $n$  and the  $n$ - $c$  interactions for all  $2n$  halo nuclei. As a three-body input, the three-body term is tuned to reproduce the experimental ground state binding energy  $B_3^{(0)}$  shown in the second column of Table I. These experimental values for the two-body and three-body energies are taken from the most recent results of the "Nuclear Data Evaluation Project" of TUNL [39], except where otherwise noted. The calculations are performed at a fixed cutoff  $\Lambda$ . Due to the Wigner bound, some care must be taken in choosing  $\Lambda$ . For the range of scattering lengths, or corresponding two-body energies, which we wish to explore, the Wigner bound leads to a maximum value for the cutoff for most of the  $2n$  halo nuclei of approximately  $\Lambda < 630$  MeV. For our calculations, we use a cutoff  $\Lambda = 580$  MeV for all nuclei. This value is significantly larger than the typical momenta in halo nuclei which are well below the pion mass.

The theoretical error for the NLO calculation is again estimated by the uncertainty of the two-body effective potential, Eq. (1), which is of order  $(r_0/a)^2$ , where  $r_0$  is the effective range of the interaction, and  $a$  the scattering length. The uncertainty in the radii is then

Nucleus	$B_3$ [keV]	$E_{nc}$ [keV]	$r_0$ [fm]	$\sqrt{\langle r_{nn}^2 \rangle}$ [fm]	$\sqrt{\langle r_{nc}^2 \rangle}$ [fm]	$\sqrt{\langle r_n^2 \rangle}$ [fm]	$\sqrt{\langle r_c^2 \rangle}$ [fm]
$^{11}\text{Li}$	247	-25	0.0	$8.7\pm 0.7$	$7.1\pm 0.5$	$6.5\pm 0.5$	$1.0\pm 0.1$
	247	-25	1.4	$8.80\pm 0.07$	$7.21\pm 0.06$	$6.51\pm 0.05$	$1.040\pm 0.008$
	247	-800 [48]	0.0	$6.8\pm 1.8$	$5.9\pm 1.5$	$5.3\pm 1.4$	$0.9\pm 0.2$
	247	-800 [48]	1.4	$6.3\pm 0.5$	$5.5\pm 0.4$	$4.9\pm 0.4$	$0.81\pm 0.06$
$^{14}\text{Be}$	1120	-200 [49]	0.0	$4.1\pm 0.5$	$3.5\pm 0.5$	$3.2\pm 0.4$	$0.40\pm 0.05$
	1120	-200 [49]	1.4	$3.86\pm 0.09$	$3.29\pm 0.08$	$3.02\pm 0.07$	$0.384\pm 0.009$
$^{12}\text{Be}$	3673	503	0.0	$3.0\pm 0.6$	$2.5\pm 0.5$	$2.3\pm 0.5$	$0.32\pm 0.07$
	3673	503	1.4	$3.3\pm 0.2$	$2.7\pm 0.1$	$2.5\pm 0.1$	$0.35\pm 0.02$
$^{18}\text{C}$	4940	731	0.0	$2.6\pm 0.7$	$2.2\pm 0.6$	$2.1\pm 0.5$	$0.18\pm 0.05$
	4940	731	1.4	$2.9\pm 0.2$	$2.4\pm 0.2$	$2.3\pm 0.2$	$0.21\pm 0.01$
$^{20}\text{C}$	3506	530 [45]	0.0	$3.0\pm 0.7$	$2.5\pm 0.6$	$2.4\pm 0.5$	$0.19\pm 0.04$
	3506	530 [45]	1.4	$3.38\pm 0.18$	$2.75\pm 0.15$	$2.60\pm 0.14$	$0.21\pm 0.01$
	3506	162	0.0	$2.8\pm 0.3$	$2.4\pm 0.3$	$2.3\pm 0.3$	$0.19\pm 0.02$
	3506	162	1.4	$3.03\pm 0.06$	$2.53\pm 0.05$	$2.39\pm 0.05$	$0.198\pm 0.004$
	3506	60	0.0	$2.8\pm 0.2$	$2.3\pm 0.2$	$2.2\pm 0.2$	$0.18\pm 0.01$
	3506	60	1.4	$2.84\pm 0.03$	$2.41\pm 0.03$	$2.28\pm 0.03$	$0.192\pm 0.002$
$^{20}\text{C}^*$	$65.0\pm 6.8$	60	0.0	$42\pm 3$	$38\pm 3$	$41\pm 3$	$2.2\pm 0.2$
$^{20}\text{C}^*$	$64.9\pm 0.7$	60	1.4	$43.2\pm 0.5$	$38.7\pm 0.4$	$42.9\pm 0.5$	$2.26\pm 0.02$

TABLE I: Various mean square radii of different halo nuclei. The second two columns show the input values for the three-body ground state energy and the two-body  $n$ - $c$  energy (negative values corresponding to virtual energies), respectively, as given by [39], except where otherwise noted. The fourth column shows the input value for both two-body effective ranges, related to LO ( $r_0 = 0.0$  fm) or NLO ( $r_0 = 1.4$  fm) calculations. The rows marked by  $^{20}\text{C}^*$  show the results for the excited Efimov state of  $^{20}\text{C}$ , with binding energy displayed in the second column, which is found above the ground state ( $B_3 = 3506$  keV).

calculated exactly as was done in the previous subsection, using the sum of the uncertainties from the  $n$ - $n$  and  $n$ - $c$  interactions:  $\Delta\langle r^2 \rangle / \langle r^2 \rangle \approx (r_{nn}/a_{nn})^2 + r_{nc}^2(2\mu_{nc}E_{nc})$ . We stress that our NLO results as well as their errors are based on our estimate of the effective range,  $r_0 = 1.4$  fm. They do not include the uncertainty in the estimate of  $r_0$  and therefore must be interpreted with some care.

We will now discuss the results for the NLO corrections to the mean square radii due to the effective range of the interactions. For the *Borromean* halo nuclei  $^{11}\text{Li}$  and  $^{14}\text{Be}$ , in which all two-body subsystems are unbound, the general tendency is for a positive effective range to shift all mean square radii to smaller values. The only exception is the case of  $^{11}\text{Li}$  using the central value of the  $n$ - $c$  energy  $E_{nc} = (-25 \pm 15)$  keV [39]. This difference is due to the fact that this value of the virtual energy is very close to the resonant limit,  $E_{nc} = 0.0$ , while the competing value  $E_{nc} = (-800 \pm 250)$  keV [48] is much larger in comparison. This can be seen more clearly if we look at the mean square radii over a range of  $E_{nc}$  values. Using the central value of the three-body binding energy as input,  $B_3^{(0)} = 247$  keV, the NLO results are plotted in comparison to the LO values in Fig. 2, with error bands estimated from the theoretical uncertainty, as described above. The solid black lines represent the LO

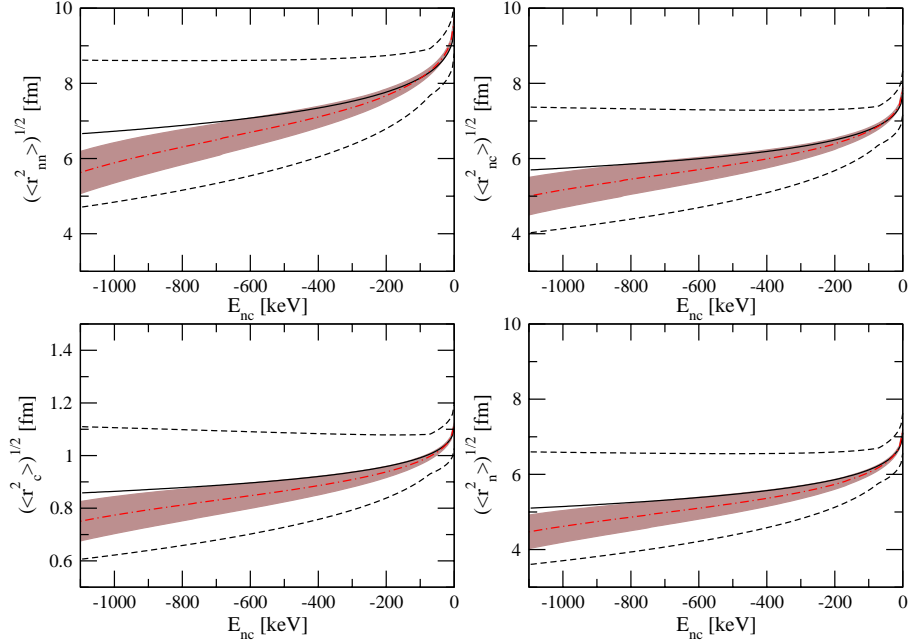


FIG. 2: The various mean square radii for  $^{11}\text{Li}$  as a function of the  $n$ - $^9\text{Li}$  two-body energy with error bands from the theoretical uncertainty. The LO results represented by the solid black lines, with error bands represented by dashed lines (as calculated in Ref. [16]). The NLO results represented by the red dotted-dashed lines with solid error bands. As input, the  $n$ - $n$  scattering length  $a_{nn} = -18.7$  fm, the three-body binding energy  $B_3^{(0)} = 247$  keV, and for NLO results the effective range  $r_0 = 1.4$  fm were used.

results, with error bands represented by the dashed lines [16]. The dotted-dashed red lines represent the NLO results, with solid colored error bands. We see that the mean square radii to NLO show the same behavior with changing  $E_{nc}$  as the LO case, with a decrease in the magnitude of  $E_{nc}$  leading to an increase in size, with a more rapid increase as the resonant limit is approached. However, for the NLO results, the increase is more rapid when  $E_{nc}$  approaches zero, such that below some value of  $|E_{nc}|$ , a positive effective range shifts the mean square radii to larger values. Otherwise, a positive effective range always shifts the mean square radii to smaller values. One can see that this shift is more drastic as the magnitude of  $|E_{nc}|$  grows larger. This is most likely due to the fact that for these large values of  $|E_{nc}|$ , the scattering length becomes smaller, nearing the order of magnitude of the effective range. For example, the virtual  $n$ - $^9\text{Li}$  energy  $E_{nc} = -1000$  keV, along with the effective range  $r_{nc} = 1.4$  fm, corresponds to a scattering length  $a_{nc} = -4.2$  fm.

The study by Marqués et al. [50] extracted experimental values for  $\sqrt{\langle r_{nn}^2 \rangle}$  for Borromean halo nuclei using the technique of intensity interferometry along with the two neutron correlation function to study the dissociation at intermediate energies of two neutrons in halo nuclei. The result for  $^{11}\text{Li}$ ,  $\sqrt{\langle r_{nn}^2 \rangle}_{exp} = (6.6 \pm 1.5)$  fm, is in close agreement with both the LO,  $\sqrt{\langle r_{nn}^2 \rangle} = (6.8 \pm 1.8)$  fm, and NLO,  $\sqrt{\langle r_{nn}^2 \rangle} = (6.3 \pm 0.5)$  fm, calculations found using the two-body virtual energy reported in [48],  $E_{nc} = -800$  keV. However, due to the large uncertainties in both the theoretical and experimental values for  $^{11}\text{Li}$ , there exists a large range of  $E_{nc}$  values which would produce a  $\sqrt{\langle r_{nn}^2 \rangle}$  value in agreement with the experimental value of Marqués et al. [50]. The LO result for  $^{14}\text{Be}$ ,  $\sqrt{\langle r_{nn}^2 \rangle} = (4.1 \pm 0.5)$  fm, is about a

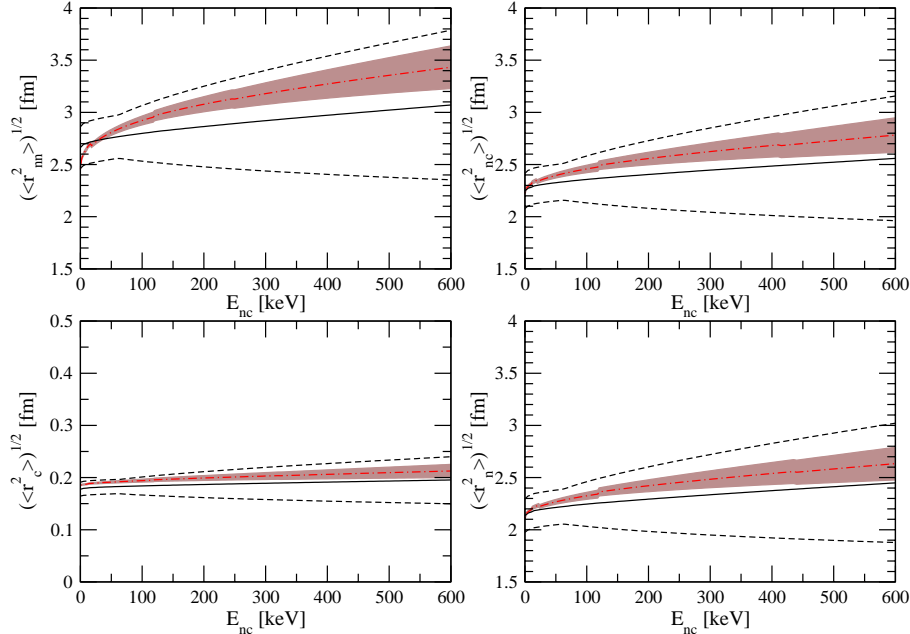


FIG. 3: The various mean square radii for  $^{20}\text{C}$  as a function of the  $n$ - $^{18}\text{C}$  two-body energy with error bands from the theoretical uncertainty. The LO results represented by the solid black lines, with error bands represented by dashed lines (as calculated in Ref. [16]). The NLO results represented by the red dotted-dashed lines with solid error bands. As input, the  $n$ - $n$  scattering length  $a_{nn} = -18.7$  fm, the three-body binding energy  $B_3^{(0)} = 3506$  keV, and for NLO results the effective range  $r_0 = 1.4$  fm were used.

Fermi below the the experimental value from Ref. [50],  $\sqrt{\langle r_{nn}^2 \rangle_{exp}} = (5.4 \pm 1.0)$  fm, but the two values are consistent within one error bar. The NLO result,  $\sqrt{\langle r_{nn}^2 \rangle} = (3.86 \pm 0.09)$  fm, is even smaller and only consistent with the experimental value within two sigma errors. Recall, however, that the NLO results are found using only an estimate for the effective ranges. Our results indicate that the effective range in the  $n$ - $^{12}\text{Be}$ -interaction is below this estimate. Furthermore, the large uncertainty in these experimental values is indicative of the need for more precise measurements of the mean square distances in  $2n$  halo nuclei. Also, the recent work by Orr [51] discusses the care which must be taken in interpreting the experimental results of [50]. Specifically, the technique is sensitive to the population of states in the continuum by the dissociation process rather than being a true ground state measurement. For more details on this issue, see Ref. [51].

Turning now to the so called *Samba* halo nuclei  $^{12}\text{Be}$ ,  $^{18}\text{C}$ , and  $^{20}\text{C}$ , for which the  $n$ - $c$  subsystem is bound, it can be seen that a positive effective range always shifts the mean square radii to larger values. We focus on the case of  $^{20}\text{C}$  and look at the mean square radii over a range of  $E_{nc}$  values. The results, using the central value for the three-body binding energy as input,  $B_3^{(0)} = 3506$  keV, were calculated to LO in Ref. [16]. We have now calculated these values to NLO, using the inverse of the pion mass as an estimate of the effective range, and the results compared to the LO case can be seen in Fig. 3, with error bands estimated from the theoretical uncertainty, as described above. The solid black lines represent the LO results, with error bands represented by the dashed lines. The dotted-dashed red lines represent the NLO results, with solid colored error bands. We see that the

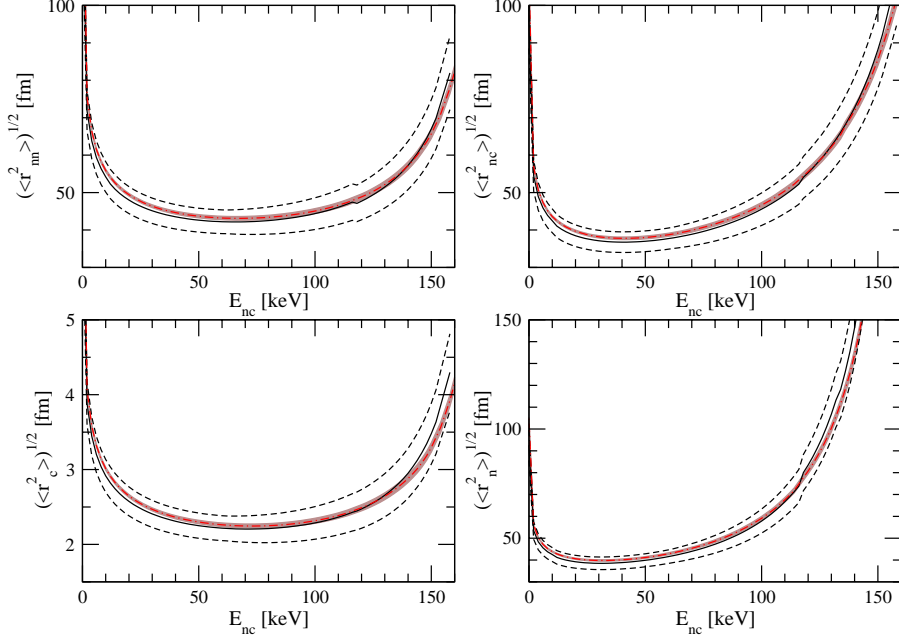


FIG. 4: The various mean square radii for the Efimov excited state of  $^{20}\text{C}$  as a function of the  $n$ - $^{18}\text{C}$  two-body energy with error bands from the theoretical uncertainty. The LO results represented by the solid black lines, with error bands represented by dashed lines (as calculated in Ref. [16]). The NLO results represented by the red dotted-dashed lines with solid error bands. As input, the  $n$ - $n$  scattering length  $a_{nn} = -18.7$  fm, the three-body binding energy  $B_3^{(0)} = 3506$  keV, and for NLO results the effective range  $r_0 = 1.4$  fm were used.

mean square radii to NLO show the same behavior with changing  $E_{nc}$  as the LO case, with an increase in  $E_{nc}$  leading to an increase in size. Also we see more clearly the general shift toward larger radii due to the effective range corrections.

As was shown in the previous subsection, there exists one Efimov excited state in  $^{20}\text{C}$  for  $E_{nc} < 165$  keV. In Fig. 4, the mean square radii for this excited state to NLO are plotted over a range of  $E_{nc}$  values, together with the LO results from Ref. [16]. Again we see that the general behavior of the mean square radii as a function of the two-body energy remains the same when calculated to NLO. At the endpoints, signifying the critical  $E_{nc}$  where the excited state breaks up, the mean square radii diverge as the excited state is destroyed and the particles fly apart. For small values of  $E_{nc}$ , there is a positive shift in the mean square radii for positive effective range, although this shift is relatively small, as compared to the relative shift in the ground state radii. However, as  $E_{nc}$  grows, there is a region where a positive effective range causes a negative shift in the mean square radii. This is related to the region where the effective range causes a positive shift in the binding energy, as described in the previous subsection.

In Table I, we have highlighted the results using two different values of the  $n$ - $c$  two-body binding energy:  $E_{nc} = (530 \pm 130)$  keV [45] and the older value  $E_{nc} = (162 \pm 112)$  keV [39]. Moreover, we show results for  $E_{nc} = 60.0$  keV which would lead to an Efimov excited state. The rows marked by  $^{20}\text{C}^*$  give the results for the excited state. The three-body binding energy of this excited state is listed in the second column with theoretical uncertainty as calculated in Sec. III A.

Within the error estimates our results generally agree with the values obtained previously by Yamashita et al. using the renormalized zero-range model [14]. Note, however, that this model does not include the effective range corrections and no error estimates are given.

Finally, we note that we explicitly do not apply our method to  ${}^6\text{He}$ . The  $n$ - ${}^4\text{He}$ -interaction is dominated by strong P-wave resonance in the  $J = 3/2$  channel, while our effective theory assumes that S-wave interactions dominate. A treatment of  ${}^6\text{He}$  therefore requires an effective theory with a different counting scheme. While various schemes to treat such P-wave resonances in Effective Field Theory have been developed [12, 13], their application to three-body systems remains to be worked out.

#### IV. CONCLUSION

In this paper, we have studied the next-to-leading order (NLO) effective range corrections to the universal properties of two-neutron halo nuclei. Our investigation was performed within an effective quantum mechanics framework using cutoffs of the order 500 MeV. Assuming that the halo nuclei have resonant S-wave interactions between the neutron and the core, the effective potential reduces to a separable S-wave potential. At NLO the potential is determined by the neutron-neutron and neutron-core energies and effective ranges plus one three-body parameter that can be fixed from any three-body datum. At next-to-next-to-leading order in the expansion in  $M_{low}/M_{high}$  no new two-body parameters enter. Whether another three-body parameter enters at this order is still an open question that has not been completely resolved [19, 21].

Our main focus was in investigating NLO corrections to the results for  $2n$  halo nuclei which arise from a non-zero effective range. Because the neutron-core effective range is not known experimentally, we were only able to estimate the range corrections assuming the effective range to be of the order of the inverse pion mass,  $r_0 \approx 1/m_\pi = 1.4$  fm. Based on this assumption, we found that the leading order results are very robust and range corrections are typically small. We investigated the possibility of excited Efimov states in halo nuclei assuming that the ground state is also an Efimov state. In particular, we found that the corrections to the parametric boundary curves, within which at least one excited Efimov state will occur were essentially unchanged for realistic values of the effective range. We found that the value of the critical  $n$ - ${}^{18}\text{C}$  two-body energy required for such an excited state to exist in  ${}^{20}\text{C}$  was decreased slightly from 165 keV at LO to 161 keV at NLO. While the TUNL nuclear data evaluation from 1995 [38, 39] quotes this energy as  $E_{nc} = (162 \pm 112)$  keV, the most recent evaluation AME2003 [44] finds  $E_{nc} = (580 \pm 100)$  keV which excludes an excited Efimov state in  ${}^{20}\text{C}$ . We also calculated the NLO shift in the excited state binding energy, finding that  $|\Delta B_3^{(1)}| < 0.5$  keV, a nearly negligible shift from the LO result.

Moreover, we calculated the shift from the LO results in the mean square radii for known  $2n$  halo nuclei. We found that for *Borromean* halo nuclei, the general tendency is for a positive effective range to shift all mean square radii to smaller values, unless the two-body  $n$ - $c$  virtual energy is very close to threshold. The opposite was found to be true for the so called *Samba* halo nuclei, for which the  $n$ - $c$  subsystem is bound. The positive effective range shifts the mean square radii of these halo nuclei to larger values. We also compared our results for the  $n$ - $n$  mean square radius to the experimental data for the Borromean halo nuclei  ${}^{11}\text{Li}$  and  ${}^{14}\text{Be}$  [50]. While there is good agreement in the  ${}^{11}\text{Li}$  system, the results for  ${}^{14}\text{Be}$  only agree within two sigma errors. This indicates that the effective range in the  $n$ - ${}^{12}\text{Be}$ -interaction is smaller than our naive estimate  $r_0 = 1.4$  fm. For a better description within our

effective theory, it will be necessary to determine the as yet unknown parameters, specifically the various neutron-core scattering lengths and effective ranges. Such information will also provide a solid basis for evaluating their universal behavior and determining the relevance of the Efimov effect as a possible binding mechanism for halo nuclei.

If the Efimov effect is responsible for the binding of at least some three-body halo nuclei or their excited states it would open the possibility of a universal binding mechanism for higher-body halo nuclei as well. In Ref. [52], a pair of universal tetramer states associated with every Efimov trimer was predicted for the case of identical bosons and their binding energies were calculated in the vicinity of the unitary limit. Recently, the spectrum of these states was mapped out for all scattering lengths and their experimental signature in 4-body recombination was pointed out [53]. Soon after this prediction, the loss resonances from both tetramers in an ultracold gas of  $^{133}\text{Cs}$  atoms were indeed observed [54]. Another calculation indicated that even higher-body cluster states with universal properties might exist [55], leading to an intriguing paradigm for a universal binding mechanism of weakly bound nuclei near the drip lines. Effective theories represent an ideal tool to explore this scenario in nuclei and predict its signatures in the structure and reactions of halo nuclei. Together with new precise experimental data from facilities such as FAIR and FRIB this will open the possibility to test this scenario. We note that this scenario does not require that the ground state of a halo nucleus is an Efimov state. More general situations where only excited states have universal character are also possible.

### Acknowledgments

We thank Gerhard Baur, Vitaly Efimov, Andreas Nogga, and Daniel Phillips for discussions. This research was supported in part by the DFG through SFB/TR 16 ‘‘Subnuclear structure of matter’’ and by the BMBF under contracts No. 06BN411 and No. 06BN9006.

### Appendix A: Wigner Bound

In this appendix, we derive the Wigner bound on the S-wave effective range for our effective potential. In the renormalization process, the bare coupling constants must be redefined twice in order to absorb high-energy effects proportional to positive powers of the cutoff parameter, which is equivalent to adding counter terms to the effective potential. The bare couplings  $\{C_0, C_2\}$  of Eq. (1) are related to the redefined couplings  $\{\tilde{C}_0, \tilde{C}_2\}$  by:

$$C_0 = \frac{\tilde{C}_0}{1 - 4\pi^2 2\mu \tilde{C}_2 \frac{2}{\pi} \frac{\Lambda^3}{3}} + \frac{2}{\pi} \frac{\Lambda^5}{5} 2\pi^2 2\mu C_2^2, \quad (\text{A1})$$

and

$$C_2 = \frac{1}{2\pi^2 2\mu \frac{2}{\pi} \frac{\Lambda^3}{3}} \left( -1 + \sqrt{\frac{1}{1 - 4\pi^2 2\mu \tilde{C}_2 \frac{2}{\pi} \frac{\Lambda^3}{3}}} \right), \quad (\text{A2})$$

where  $\mu$  is the two-body reduced mass. One clearly sees that there are real values of  $\tilde{C}_2$  for which the bare couplings become complex. This would imply a complex effective potential.

Therefore, we must place a constraint on the value of  $\tilde{C}_2$ :

$$4\pi^2 2\mu \tilde{C}_2 \frac{2}{\pi} \frac{\Lambda^3}{3} \leq 1. \quad (\text{A3})$$

The renormalization of the effective potential is completed by tuning the redefined coupling constants to reproduce the scattering length  $a$  and the effective range  $r_0$  according to the following expressions:

$$\frac{1}{\tilde{C}_0} = 2\pi^2 2\mu \left[ \frac{1}{a} f(\tilde{x}_0) - \frac{2}{\pi} \Lambda \right], \quad (\text{A4})$$

and

$$\tilde{C}_2 = \frac{1}{4\pi^2 2\mu} \left[ \frac{\frac{r_0}{2} f(\tilde{x}_0) - \frac{2}{\pi} \frac{1}{\Lambda}}{\left( \frac{1}{a} f(\tilde{x}_0) - \frac{2}{\pi} \Lambda \right)^2} \right], \quad (\text{A5})$$

where the parameter  $\tilde{x}_0$  is analogous to  $\tilde{x}_{ni}$  from Eq. (10) found with  $a_{ni} = a$  and  $r_{ni} = r_0$ . Substituting Eq. (A5) into Eq. (A3), we find the Wigner bound for our effective potential:

$$\frac{2}{\pi} \frac{\Lambda^3}{3} \frac{\frac{r_0}{2} f(\tilde{x}_0) - \frac{2}{\pi} \frac{1}{\Lambda}}{\left( \frac{1}{a} f(\tilde{x}_0) - \frac{2}{\pi} \Lambda \right)^2} \leq 1. \quad (\text{A6})$$

If the cutoff is much larger than the momentum scale of the T-matrix pole,  $\Lambda \gg \sqrt{2\mu E_2}$ , then  $f(\tilde{x}_0) \rightarrow 1$  and we have:

$$r_0 \leq 2 \left( \frac{2}{\pi} \frac{4}{\Lambda} - \frac{6}{a\Lambda^2} + \frac{\pi}{2} \frac{3}{a^2\Lambda^3} \right). \quad (\text{A7})$$

It is then obvious that for  $\Lambda \rightarrow \infty$ , the effective range must be equal to or less than zero. Conversely, by setting the input values of the scattering length and effective range, Eq. (A6) places a constraint on the maximum value of the cutoff  $\Lambda$ .

## Appendix B: Wave function and matter density form factors

The full bound state wave function of a two-neutron halo nucleus can be reconstructed from the solutions for the spectator functions  $F_n$  and  $F_c$  found from the coupled integral equations (2, 3). The form of the wave function,  ${}_i\langle pq|\Psi\rangle \equiv \Psi_i(p, q)$ , depends on the choice of two-body subsystem and corresponding spectator particle, where the index  $i = n, c$  labels the spectator particle. Recall that in the wave functions, the Jacobi momentum  $p$  describes the relative momentum between the two particles in the chosen two-body subsystem, while  $q$  describes the momentum of the spectator particle relative to the center of mass of the two-body subsystem.

To reconstruct the S-wave part of the full wave functions with either a neutron or core



spectator from the spectator functions we find:

$$\begin{aligned} \Psi_n(p, q) = & \left( G_0^n(p, q; B_3) + \frac{H(\Lambda)}{\Lambda^2} \right) \left[ t_n(q; B_3) F_n(q) \right. \\ & \left. + \frac{1}{2} \int_{-1}^1 dx t_n(\tilde{\pi}'_{nn}; B_3) F_n(\tilde{\pi}'_{nn}) + t_c(\tilde{\pi}'_{nc}; B_3) F_c(\tilde{\pi}'_{nc}) \right], \end{aligned} \quad (\text{B1})$$

$$\begin{aligned} \Psi_c(p, q) = & \left( G_0^c(p, q; B_3) + \frac{H(\Lambda)}{\Lambda^2} \right) \left[ t_c(q; B_3) F_c(q) \right. \\ & \left. + \int_{-1}^1 dx t_n(\tilde{\pi}'_{cn}; B_3) F_n(\tilde{\pi}'_{cn}) \right], \end{aligned} \quad (\text{B2})$$

where the two-body T-matrices  $t_n$  and  $t_c$  are given in Eqs. (6, 8). The expressions for the propagators  $G_0^n$  and  $G_0^c$  are:

$$G_0^n(p, q; B_3) = \left[ B_3 + \frac{A+1}{2A} p^2 + \frac{A+2}{2(A+1)} q^2 \right]^{-1}, \quad (\text{B3})$$

$$G_0^c(p, q; B_3) = \left[ B_3 + p^2 + \frac{A+2}{4A} q^2 \right]^{-1}. \quad (\text{B4})$$

Finally, the shifted momenta are:

$$\tilde{\pi}'_{nn} \equiv \tilde{\pi}'_{nn}(p, q) = \sqrt{p^2 + \frac{1}{(A+1)^2} q^2 - \frac{1}{A+1} 2pqx}, \quad (\text{B5})$$

$$\tilde{\pi}'_{nc} \equiv \tilde{\pi}'_{nc}(p, q) = \sqrt{p^2 + \frac{A^2}{(A+1)^2} q^2 - \frac{A}{A+1} 2pqx}, \quad (\text{B6})$$

and

$$\tilde{\pi}'_{cn} \equiv \tilde{\pi}'_{cn}(p, q) = \sqrt{p^2 + \frac{1}{4} q^2 - pqx}. \quad (\text{B7})$$

The three-body wave functions can be used to calculate other low-energy properties of the three-body bound state. With the Jacobi momentum states it is straightforward to calculate the Fourier transform of the one- and two-body matter densities with respect to the momentum transfer squared. These are defined as the one- and two-body matter density form factors  $\mathcal{F}_i(k^2)$  and  $\mathcal{F}_{ni}(k^2)$ , respectively, where  $i = n, c$ . The derivation of the form factors from the three-body S-wave wave functions can be found in Refs. [16, 29]. The resulting expression for the one-body form factors is:

$$\mathcal{F}_i(k^2) = \int dp p^2 \int dq q^2 \int_{-1}^1 dx \Psi_i(p, q) \Psi_i(p, \sqrt{q^2 + k^2 - 2qkx}), \quad (\text{B8})$$

while the two-body form factors are:

$$\mathcal{F}_{nc}(k^2) = \int dp p^2 \int dq q^2 \int_{-1}^1 dx \Psi_n(p, q) \Psi_n(\sqrt{p^2 + k^2 - 2pkx}, q), \quad (\text{B9})$$

and

$$\mathcal{F}_{nn}(k^2) = \int dp p^2 \int dq q^2 \int_{-1}^1 dx \Psi_c(p, q) \Psi_c(\sqrt{p^2 + k^2 - 2pkx}, q). \quad (\text{B10})$$

- 
- [1] P.F. Bedaque and U. van Kolck, *Ann. Rev. Nucl. Part. Sci.* **52** (2002) 339 [arXiv:nucl-th/0203055].
  - [2] E. Braaten and H.-W. Hammer, *Phys. Rept.* **428** (2006) 259 [arXiv:cond-mat/0410417].
  - [3] E. Epelbaum, H.-W. Hammer and U.-G. Meißner, *Rev. Mod. Phys.* **81** (2009) 1773 [arXiv:0811.1338 [nucl-th]].
  - [4] L. Platter, *Few-Body Syst.* **46** (2009) 139, [arXiv:0904.2227].
  - [5] K. Riisager, *Rev. Mod. Phys.* **66** (1994) 1105.
  - [6] M.V. Zhukov, B.V. Danilin, D.V. Fedorov, J.M. Bang, I.J. Thompson, and J.S. Vaagen, *Phys. Rep.* **231** (1993) 151.
  - [7] P.G. Hansen, A.S. Jensen, and B. Jonson, *Ann. Rev. Nucl. Part. Sci.* **45** (1995) 591.
  - [8] A.S. Jensen, K. Riisager, D.V. Fedorov, and E. Garrido, *Rev. Mod. Phys.* **76** (2004) 215.
  - [9] D.V. Fedorov, A.S. Jensen and K. Riisager, *Phys. Rev. Lett.* **73** (1994) 2817 [arXiv:nucl-th/9409018].
  - [10] A.E.A. Amorim, T. Frederico and L. Tomio, *Phys. Rev. C* **56** (1997) R2378 [arXiv:nucl-th/9708023].
  - [11] I. Mazumdar, V. Arora, and V. S. Bhasin, *Phys. Rev. C* **61** (2000) R051303.
  - [12] C.A. Bertulani, H.-W. Hammer and U. Van Kolck, *Nucl. Phys. A* **712** (2002) 37 [arXiv:nucl-th/0205063].
  - [13] P.F. Bedaque, H.-W. Hammer and U. van Kolck, *Phys. Lett. B* **569** (2003) 159 [arXiv:nucl-th/0304007].
  - [14] M. T. Yamashita, L. Tomio and T. Frederico, *Nucl. Phys. A* **735** (2004) 40 [arXiv:nucl-th/0401063].
  - [15] R. Higa, H.-W. Hammer and U. van Kolck, *Nucl. Phys. A* **809** (2008) 171 [arXiv:0802.3426 [nucl-th]].
  - [16] D. L. Canham and H.-W. Hammer, *Eur. Phys. J. A* **37** (2008) 367 [arXiv:0807.3258 [nucl-th]].
  - [17] V. Efimov, *Phys. Lett.* **33B** (1970) 563.
  - [18] H.-W. Hammer and T. Mehen, *Phys. Lett. B* **516** (2001) 353. [arXiv:nucl-th/0105072].
  - [19] P.F. Bedaque, G. Rupak, H.W. Griebhammer, and H.-W. Hammer, *Nucl. Phys. A* **714** (2003) 589 [arXiv:nucl-th/0207034].
  - [20] H.W. Griebhammer, *Nucl. Phys. A* **744** (2004) 192 [arXiv:nucl-th/0404073].
  - [21] L. Platter, *Phys. Rev. C* **74** (2006) 037001 [arXiv:nucl-th/0606006].
  - [22] J. Kirscher, H.W. Griebhammer, D. Shukla and H. M. Hofmann, arXiv:0903.5538 [nucl-th].
  - [23] M. Thøgersen, D.V. Fedorov and A.S. Jensen, *Phys. Rev. A* **78** (2008) 020501.
  - [24] L. Platter, C. Ji and D. R. Phillips, *Phys. Rev. A* **79** (2009) 022702 [arXiv:0808.1230 [cond-mat.other]].
  - [25] L. Platter, H.-W. Hammer and U.-G. Meißner, *Phys. Rev. A* **70** (2004) 052101 [arXiv:cond-mat/0404313].
  - [26] J.A. Wheeler, *Phys. Rev.* **52** (1937) 1083.
  - [27] T. Neff and H. Feldmeier, *Nucl. Phys. A* **738** (2004) 357 [arXiv:nucl-th/0312130].

- [28] H. Kamada, S. Oryu and A. Nogga, Phys. Rev. C **62** (2000) 034004 [arXiv:nucl-th/0001005].
- [29] D.L. Canham, Ph.D. Thesis, University of Bonn (2009), URN: urn:nbn:de:hbz:5N-17947.
- [30] P.F. Bedaque, H.-W. Hammer, and U. van Kolck, Phys. Rev. Lett. **82** (1999) 463 [arXiv:nucl-th/9809025].
- [31] H.-W. Hammer and T. Mehen, Nucl. Phys. A **690** (2001) 535 [arXiv:nucl-th/0011024].
- [32] G.A. Miller, B.M.K. Nefkens and I. Slaus, Phys. Rept. **194** (1990) 1.
- [33] D.R. Phillips, S.R. Beane and T.D. Cohen, Annals Phys. **263** (1998) 255 [arXiv:hep-th/9706070].
- [34] E.P. Wigner, Phys. Rev. **98** (1955) 145.
- [35] D.R. Phillips and T.D. Cohen, Phys. Lett. B **390** (1997) 7 [arXiv:nucl-th/9607048].
- [36] H.-W. Hammer and D. Lee, Phys. Lett. B **681** (2009) 500 [arXiv:0907.1763 [nucl-th]].
- [37] D.E. Gonzales Trotter *et al.*, Phys. Rev. Lett. **83** (1999) 3788.
- [38] G. Audi and A.H. Wapstra, Nucl. Phys. A **595** (1995) 409.
- [39] TUNL nuclear data evaluation project: <http://www.tunl.duke.edu/NuclData/>.
- [40] D.J. Viera *et al.*, Phys. Rev. Lett. **57** (1986) 3253.
- [41] A. Gillebert *et al.*, Phys. Lett. B **192** (1987) 39.
- [42] J.M. Wouters *et al.*, Z. Phys. A **331** (1988) 229.
- [43] N.A. Orr *et al.*, Phys. Lett. B **258** (1991) 29.
- [44] G. Audi, A.H. Wapstra and C. Thibault, Nucl. Phys. A **729** (2003) 337.
- [45] T. Nakamura *et al.*, Phys. Rev. Lett. **83** (1999) 1112.
- [46] S. Typel and G. Baur, Phys. Rev. Lett. **93** (2004) 142502.
- [47] T. Aumann, Eur. Phys. J. A **26** (2005) 441.
- [48] K.H. Wilcox *et al.*, Phys. Lett. **59B** (1975) 142.
- [49] M. Thoennessen, S. Yokoyama, P. G. Hansen, Phys. Rev. C **63** (2000) 014308.
- [50] F.M. Marqués *et al.*, Phys. Lett. B **476** (2000) 219; Phys. Rev. C **64** (2001) 061301.
- [51] N.A. Orr, arXiv:0803.0886 [nucl-ex].
- [52] H.-W. Hammer and L. Platter, Eur. Phys. J. A **32** (2007) 113 [arXiv:nucl-th/0610105].
- [53] J. von Stecher, J. P. D’Incao, and C. H. Greene, Nature Physics **5** (2009) 417 [arXiv:0810.3876].
- [54] F. Ferlaino, S. Knoop, M. Berninger, W. Harm, J. P. D’Incao, H.-C. Nägerl, R. Grimm, Phys. Rev. Lett. **102** (2009) 140401 [arXiv:0903.1276].
- [55] J. von Stecher, arXiv:0909.4056 [cond-mat.quant-gas].